

Spectral Domain Optical Coherence Tomography in Awake Rabbits Allows Identification of the Visual Streak, a Comparison with Histology

Arnold Lavaud¹, Petr Soukup¹, Louise Martin², Sonja Hartnack³, and Simon Pot¹

¹ Ophthalmology Section, Equine Department, Vetsuisse Faculty, University of Zurich, Zurich, Switzerland

² Clinic for Zoo Animals, Exotic Pets and Wildlife, Vetsuisse Faculty, University of Zurich, Zurich, Switzerland

³ Section of Epidemiology, Vetsuisse Faculty, University of Zurich, Zurich, Switzerland

Correspondence: Simon Pot, Ophthalmology Section, Vetsuisse Faculty, University of Zurich, Winterthurerstrasse 260, 8057 Zurich, Switzerland. e-mail: spot@vetclinics.uzh.ch

Received: October 8, 2019

Accepted: February 13, 2020

Published: April 23, 2020

Keywords: optical coherence tomography; SD-OCT; histology; visual streak; outer retina; rabbit; photoreceptors

Citation: Lavaud A, Soukup P, Martin L, Hartnack S, Pot S. Spectral domain optical coherence tomography in awake rabbits allows identification of the visual streak, a comparison with histology. *Trans Vis Sci Tech.* 2020;9(5):13, <https://doi.org/10.1167/tvst.9.5.13>

Purpose: To evaluate visual streak (VS) identification on spectral-domain optical coherence tomography (SD-OCT) scans in awake rabbits. To report thickness measurements in the VS and adjacent retina on OCT B-scans and histologic sections and to assess inter-method bias, precision and repeatability between OCT and histology.

Methods: Vertical SD-OCT B-scan images through the optic nerve head and VS were acquired from 16 awake, ophthalmologically healthy experimental rabbits. Scans were acquired from both eyes, which were later enucleated and processed for light microscopy. Inner retina, inner nuclear layer, outer nuclear layer, outer retina (OR) and photoreceptor outer segment (PROS) thickness were measured on OCT images and digitalized microscopy slides in- and outside of the VS, and compared using linear mixed effects models.

Results: Both SD-OCT and histology allowed retinal layer identification and measurement. On OCT, OR and PROS were thickest in the central VS and thinnest outside the VS. Histology mirrored OCT results for central outer retinal layers but shows discrepancies for other layers likely because of postmortem processing artifacts. The method comparison demonstrated better repeatability for OCT measurements compared with histology.

Conclusions: Increased OR and PROS thickness compared with the adjacent retina allowed identification of the VS on SD-OCT in awake rabbits. OCT allows measurements devoid of processing artifacts in contrast to histology.

Translational Relevance: SD-OCT is possible in awake rabbits. Easy and reliable identification of the VS may facilitate the positioning and use of rabbits as model species in human macular and generalized retinal disease research

Introduction

Rabbits are known to have a visual streak (VS), where the rod and cone photoreceptor, ganglion cell and amacrine cell density is highest, and which is located roughly 3 mm ventral to the optic nerve head (ONH).^{1–5} The rabbit is a frequently used animal model in ophthalmology research because the size of the rabbit eye is similar to that of humans and because rabbits present breeding, handling, cost-technical, and regulatory advantages over other mammals.⁶ A mid-sized animal model like a rabbit is therefore of partic-

ular importance for testing new therapeutic interventions. In contrast with rodent models, rabbits are very useful for studying retinal degenerative diseases due to the fact that a VS is present.^{7–11} In addition, there is a considerable accumulation of previous work on the anatomy and physiology of the rabbit retina.^{1,2,4,12–19}

Optical coherence tomography (OCT) is a noninvasive transpupillary imaging technology that produces high-quality images of the retina and the optic nerve and allows quantitative measurements of retinal thickness. Spectral-domain OCT (SD-OCT) has enabled high-speed scanning and improved image resolution.^{20,21} In the past decade, SD-OCT images have

shown excellent morphologic agreement with histological sections in humans and different animal models.^{21–35} Therefore, OCT is sometimes described as “in vivo microscopy.”^{26,36,37} SD-OCT imaging allows evaluation of the junction between photoreceptor inner and outer segments^{38–40} and of the external limiting membrane (ELM)^{40–42} as hallmarks of photoreceptor integrity in human patients. In animal experiments, SD-OCT may allow real time in vivo imaging of retinal architecture modifications that affect photoreceptor integrity and retinal function and allows the follow-up of a single subject without sacrificing animals at interim timepoints.^{43,44}

The use of SD-OCT for the quantification of normal rabbit retinal anatomy has been reported in a number of studies but only in anesthetized animals.^{45–47} In animals, it is generally recommended to resort to general anesthesia to ensure that the subject is adequately immobilized and motion artifacts are limited.⁴⁸ Moreover, none of these studies evaluated the thickness of different retinal layers at locations inside and outside of the VS. Therefore, geographic variations in retinal layer thickness across the rabbit retina on SD-OCT have not been evaluated. Scrutiny of published OCT images^{43,49} and personal observations based on our own OCT library led us to hypothesize that identification and evaluation of the VS should be possible on SD-OCT images obtained from awake rabbits. The purpose of this study is therefore twofold. To evaluate VS identification on SD-OCT B-scans from awake experimental rabbits. To report quantitative SD-OCT B-scan measurements of the VS and adjacent retinal regions and compare those with measurements obtained from histologic sections to assess inter-method bias, precision and repeatability between OCT and histology.

Methods

Animals

This study was conducted, and the animals were treated, in accordance with the guidelines of the Association for Research in Vision and Ophthalmology (ARVO) Statement for the Use of Animals in Ophthalmic and Vision Research. All experiments were approved by the committee on animal experimentation of the Cantonal Veterinary Office Zurich (license numbers ZH204/17 and ZH241/17) and performed according to the ethics and animal experimentation bylaws of the Vetsuisse Faculty, University of Zurich, Switzerland. Eight male and eight female, clinically healthy, 8-month-old, commercially crossbred

pigmented New Zealand/California rabbits, weighing approximately 4.3 ± 0.245 kg, were used in this study. All animals underwent a complete ocular examination (intraocular pressure [IOP] evaluation via rebound tonometry, slit-lamp biomicroscopy, fluorescein staining, indirect ophthalmoscopy) to rule out the presence of ocular diseases prior to inclusion in this study. The pupils were dilated with topical 1% tropicamide eyedrops (Thea Pharma SA, Schaffhausen, Switzerland).

SD-OCT Image Acquisition

Images were obtained from awake animals using minimal manual restraint by gently holding and wrapping the animals in a towel. A commercially available high-resolution SD-OCT instrument with an axial pixel resolution of 2.4 μm (Biotigen Envisu R2210 SD-OCT; Leica Microsystems, Wetzlar, Germany) equipped with a General Retina lens (Biotigen Envisu) was used to image the retina and optic nerve in all animals. To obtain cross-sectional images through the VS the following scans were obtained: vertical volume scans (12×12 mm, 100 B-scans and 1000 A-scans per B-scan) centered on the VS, approximately 3 mm ventral to the lower ONH rim (Fig. 1A); vertical linear scans (10 mm, 1000 A-scans per B-scan, 5 B-scans averaged) passing either through the center of the ONH or the nasal ONH rim and including the VS (Fig. 1B).

Histology Evaluation

The rabbits were euthanized for reasons unrelated to the study presented here. Eyes were enucleated immediately postmortem and marked with sutures to facilitate orientation.

Paraffin-embedded Samples

Eyes from 14 animals were fixed by immersion in Davidson's fixative solution (A3200, AppliChem, Darmstadt, Germany) for 48 hours followed by an additional 24-hour immersion in 70% ethanol (Hanseler Swiss Pharma, Herisau, Switzerland). A vertical plane of section was used to bisect the fixed globes.⁵⁰ To achieve perfect perpendicular orientation of the tissue specimens in the cassettes during histology processing and thus ensure the correct localization of the histology sections when compared to OCTs, the temporal ONH was “sacrificed” and therefore could not be sectioned and measured. The decision to sacrifice the temporal, and not the nasal, ONH was arbitrary. The nasal hemisections were processed into paraffin blocks via standard automated dehydration

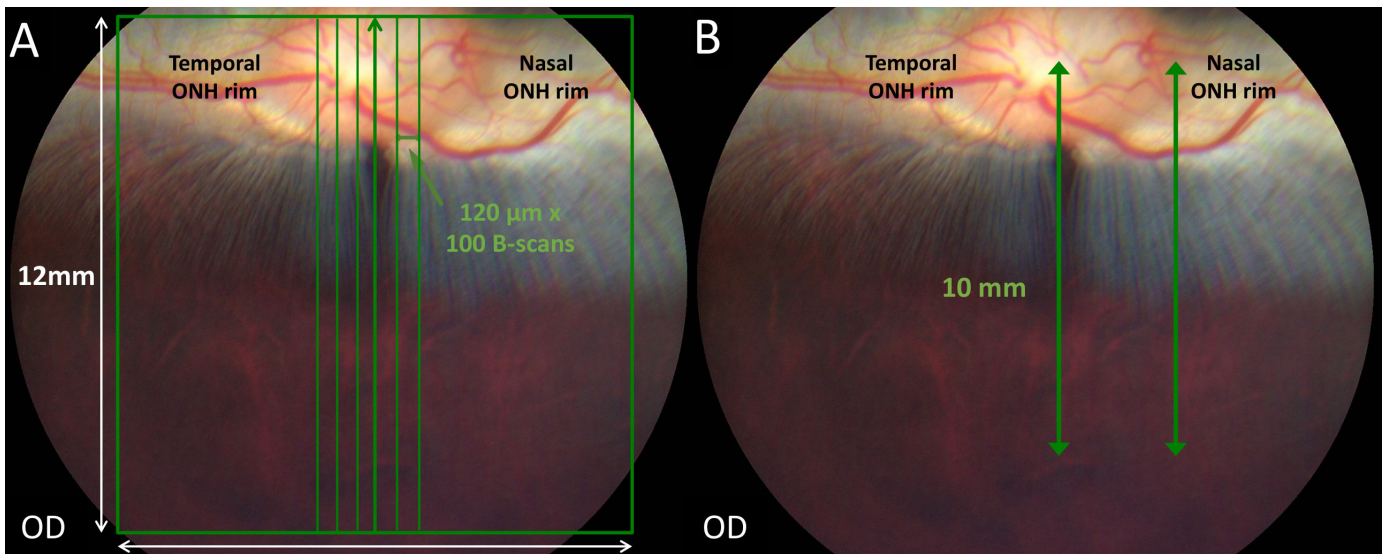


Figure 1. SD-OCT image acquisition methodology. Color fundus pictures of a crossbred pigmented New Zealand/California rabbit. (A) A volume scan mode was used to obtain cross-sectional retinal images. The green square represents a volume scan including the visual streak ventral to the optic disc (100 vertical B-scans separated by 120 μm in a field of 12 \times 12 mm). (B) A linear scan mode was used to obtain vertical line scans (10-mm scan length, 5 B-scans averaged) passing through the center of the ONH or the nasal rim of the ONH, perpendicular to the main retinal medullary rays and including the visual streak.

and paraffin-embedding (Tissue-Tek VIP 5, Sakura, Alphen aan den Rijn, The Netherlands). Sections were obtained by trimming the blocks to reach the middle of the optic nerve head where eight central sections were obtained. Next, the blocks were trimmed to the nasal ONH rim where eight nasal sections were obtained. All sections were 4.5 μm thick, stained with hematoxylin-eosin, and evaluated using a light microscope (Zeiss AxioScope A1, Carl Zeiss, Feldbach, Switzerland). The four best central and nasal sections were selected to be scanned at 40 \times magnification (Aperio Scanscope AT, Leica Biosystems, Nussloch, Germany) for digitized measurement collection.

Resin-embedded Samples

Eyes from two animals were enucleated immediately post-mortem and fixed in 3% glutaraldehyde in 0.1M sodium cacodylate buffer (EMS-16120, Electron Microscopy Sciences, Hatfield, PA, USA). A small fenestration was made at the limbus and pars plana using microsurgical tools after 60 minutes of fixation to facilitate fixative penetration and optimize fixation of the retina and underlying choroid. Separate samples were obtained from the center and nasal periphery of the ONH and trimmed to include the ONH and the visual streak area. Samples were then processed manually and embedded in epoxy resin (45359, Sigma-Aldrich, Saint Louis, MO, USA). Subsequently, the nasal block from one of the rabbits for which a total retinal thickness (TRT) and an outer retina (OR) thick-

ness topography was constructed was cut by ultramicrotome (UC7, Leica) into semithin sections (750 μm thickness) at 500- μm intervals covering the distance from the ventral ONH rim to the sample edge at 4 mm ventral to the ONH rim. All sections were stained with toluidine blue and qualitatively evaluated with estimation of photoreceptor outer segment (PROS) and OR length using light microscopy (Olympus BX-53 microscope equipped with 100x UPlanFN L 1.3 oil and 20x UPlanFN L 0.5 objectives).

Evaluation and Measurement Protocols

Thickness measurements of the following five different retinal layers and zones of interest were collected from SD-OCT B-scan images and hematoxylin-eosin stained histology sections. The inner retina (IR) was defined as the linear distance between the internal limiting membrane (ILM) and ELM. The OR was defined as the linear distance between ELM and the choriocapillaris (CC), including the retinal pigment epithelium/Bruch's membrane complex (RPE/BM). The inner nuclear layer (INL) and outer nuclear layer (ONL) were measured. The PROS length was defined as the hyporeflective photoreceptor outer segment (OS) band plus the hyperreflective interdigitation zone (IZ) band on OCT, thus excluding the ellipsoid zone (EZ), and RPE/BM bands. On histology, PROS length was defined as the linear distance between the interface of inner and outer photoreceptor segments and the

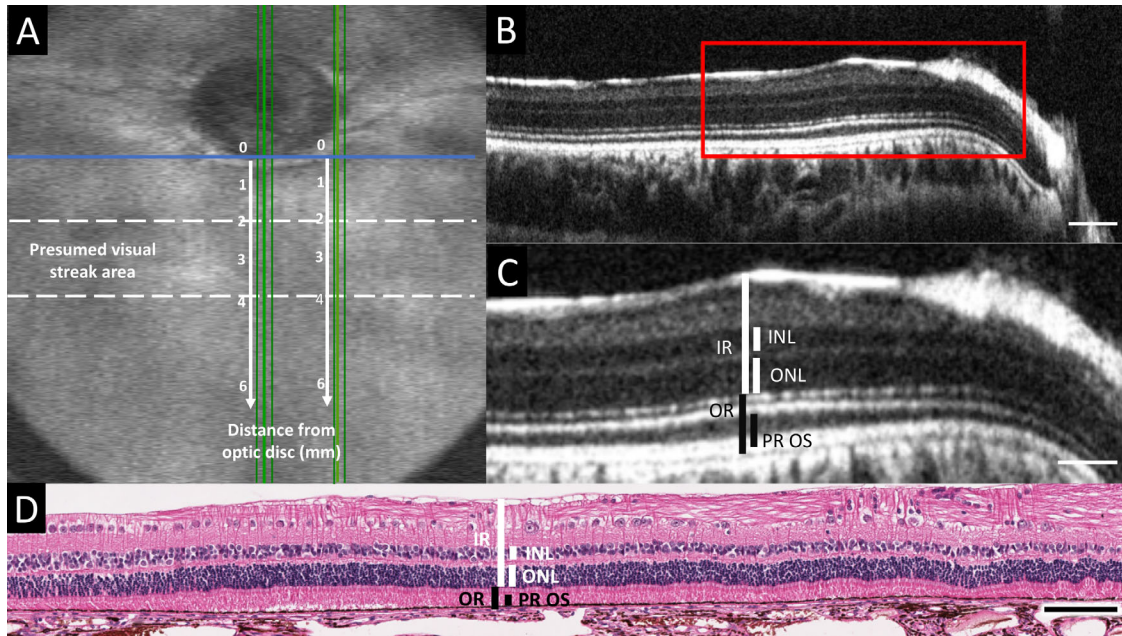


Figure 2. Retinal thickness measurement methodology. (A) OCT volume intensity projection providing an overview of a rabbit fundus, including the optic nerve head (ONH) and presumed visual streak area (between dotted lines). Retinal thickness measurements were collected from vertical OCT scans and histologic sections passing through the center and the nasal rim of the ONH (vertical green lines). For each location, the measurements were repeated at five different positions at 1, 2, 3, 4, and 6 mm ventral to the ONH rim (vertical white arrows and numbers). A horizontal line parallel to the ventral rim at the center of the ONH (horizontal blue line) was taken as zero-position benchmark for both central and nasal measurements. (B) Vertical SD-OCT B-scan image along one of the green lines (replicates) passing through the center of the ONH in panel A. (C) Magnified B-scan image of the area indicated by the red rectangle in panel B, including the visual streak. The retinal thickness measurements collected from OCT B-scan images and histology sections are indicated in white for the inner retinal layers and in black for the outer retinal layers. IR (inner retina): linear distance between internal limiting membrane (ILM) and external limiting membrane (ELM); INL (inner nuclear layer); ONL (outer nuclear layer); OR (outer retina): linear distance between ELM and the choriocapillaris (CC); PROS (photoreceptor outer segment length): hyporeflective photoreceptor outer segment (OS) band + hyperreflective interdigitation zone (IZ) band on OCT, linear distance between the interface of inner and outer photoreceptor segments and the surface of the RPE on histology. (D) Hematoxylin-eosin stained retinal section corresponding to the area depicted by the OCT image in panel C. Scale bar = 100 μm (B), 50 μm (C), and 100 μm (D)

surface of the RPE. The thickness of each layer/zone was measured at five different positions at 1, 2, 3, 4, and 6 mm ventral to the central ONH rim. These measurement positions were selected based on the previously published localization of the center of the rabbit VS at roughly 3 mm ventral to the ONH rim.^{1,2} These measurements were collected from the vertical scans and sections passing through the center and the nasal rim of the ONH (Fig. 2A). To allow comparison of central and nasal measurements from the 1, 2, 3, 4, and 6 mm positions ventral to the ONH rim a horizontal line parallel to the ventral rim at the center of the ONH was taken as zero-position benchmark for both central and nasal measurements. Acquired SD-OCT images were processed with ImageJ software.⁵¹ Retinal layer/zone thicknesses were measured manually and the identification of the different retinal layers/zones was based on those previously described in humans with the use of SD-OCT (illustrated in Supplementary Figure S1).⁴⁰ The measurements were repeated on four repli-

cate central and nasal scans for each eye (one linear scan and three successive volume scan lines). To be consistent with the localization of the OCT measurements, four histological sections (replicates) closest to the nasal rim and to the center of the ONH were used for analysis. Measurements were performed manually using slide viewing software (ViewPoint 1.0.0.9442, PreciPoint, Freising, Germany).

Manually assisted segmentation of selected OCT volume scans from three rabbits was performed using the segmentation software OCTseg (Version 0.4, M.Mayer, University of Erlangen-Nuremberg, Nuremberg, Germany).⁵² Three lines were segmented on each single OCT B-scan in the selected volumes: the ILM-vitreous interface, ELM line, and RPE/BM-choriocapillaris interface. Topographic maps illustrating TRT and OR thickness across the ventral retina were generated from the segmentation values using ParaView data visualization software (Version 5.6.0, Kitware Inc., Clifton Park, NY,

USA) and projected onto OCT volume intensity projections.

Manual cell counting was performed on hematoxylin-eosin stained histology sections passing through the central ONH using 40× magnification. Numbers of rows of INL and ONL nuclei and the number of ganglion cells (GC) were counted at the 1, 2, 3, 4, and 6 mm positions ventral to the ONH rim, corresponding to the thickness measurement locations.

Statistical Analysis

With the aim to assess if the retinal thickness measurements differed significantly between positions ventral to the ONH rim and for both locations, central and nasal, linear mixed effects models were applied. Eyes nested within animals were included as random effect. Distance from the ventral ONH rim and replicates were included as fixed effects. Model selection was based on likelihood ratio tests. Adjustment for multiple comparisons was done with Tukey's approach available in the packages `multcomp`⁵³ and `nlme`⁵⁴ in the software R.⁵⁵ The resulting estimated thicknesses of the different layers are presented in the form of 95% confidence intervals. Regarding the cell counting the same approach was used. Linear mixed effects models using Tukey's multiple comparisons were applied to assess if INL and ONL nuclei row and GC numbers differed significantly between positions ventral to the ONH rim for the central location.

For the method comparison studies, similar to Roy,⁵⁶ four linear mixed effects models (one reference and three nested models) with different between-subject variances (precision) and within-subject variances (repeatability) were performed with the aim to assess a potential inter-method bias, precision and repeatability. The null hypothesis stated that the measurement means (inter-method bias), between-subject variance (precision) and within-subject variance (repeatability) are equal for both measurement methods. The null hypothesis was rejected at $P < 0.05$. According to Bland and Altman,⁵⁷ the repeatability coefficients are $1.96\sqrt{2} * \sigma_e$, where σ_e represents the within-subject variance determined by the residual standard deviation of the random effects, possibly multiplied with a factor indicating the different standard deviations per method.^{56,57}

Results

Visualization of Retinal Structures

SD-OCT. Vertically oriented OCT B-scan images through the nasal rim or the center of the ONH permit-

ted clear separation and identification of the outer retinal layers in all 16 rabbits scanned awake. ELM, EZ, OS, IZ, and RPE/BM complex were clearly identifiable allowing measurements of OR and PROS. Although SD-OCT allowed observation of all inner retinal layers in most of the cases, occasionally the outer plexiform layer could not be visualized because of low contrast, which prevented INL and ONL measurements in 7.7% (43/560) of central and 10.2% (57/560) of nasal replicate measurement positions, respectively.

Paraffin-embedded sample histology. Four eyes were excluded from further evaluation after processing due to large scale fixation artifacts in the VS area. The presence of artifactual retinal detachments or slight crushing of the PR outer segments in eyes with an otherwise well-preserved anatomy (illustrated in Supplementary Figure S2) prevented OR and PROS measurements in 7.3% (35/480) of central and 6.2% (30/480) of nasal replicates, respectively. Other processing artifacts or slightly oblique sectioning prevented IR, INL, and ONL measurements in 1% (5/480) of central and 6.2% (30/480) of nasal replicate measurement positions, respectively.

Retinal thickness measurements

All retinal thickness measurements obtained at 1, 2, 3, 4, and 6 mm ventral to the lower ONH rim in the central and nasal ONH locations are presented as Boxplots in Figures 3 and 4, respectively. Numerical values of the same datasets and corresponding P values for all comparisons are presented in Supplementary Tables S1a and S1b for the SD-OCT B-scan images and in Supplementary Tables S2a and S2b for the histology sections.

Outer Retinal Layers

Both OR and PROS measured on OCT at the central and nasal ONH demonstrated a statistically significant greater thickness within the VS, (at 2, 3, and 4 mm ventral to the ONH) compared with outside the VS (at 1 and 6 mm). Within the VS, OR and PROS were thickest in the center of the VS at 3 mm ventral to the ONH, compared with at 2 and 4 mm.

Histology-derived OR and PROS thickness measurements at the center of the ONH mirrored the OCT-derived measurements with the OR and PROS being the thickest in the center of the VS and thinnest outside the VS. Within the VS, OR and PROS were significantly thicker at 2 mm compared with 4 mm ventral to the ONH, which was the opposite for the OCT-derived measurements. Overall, all layers were significantly thinner on histology compared to OCT.

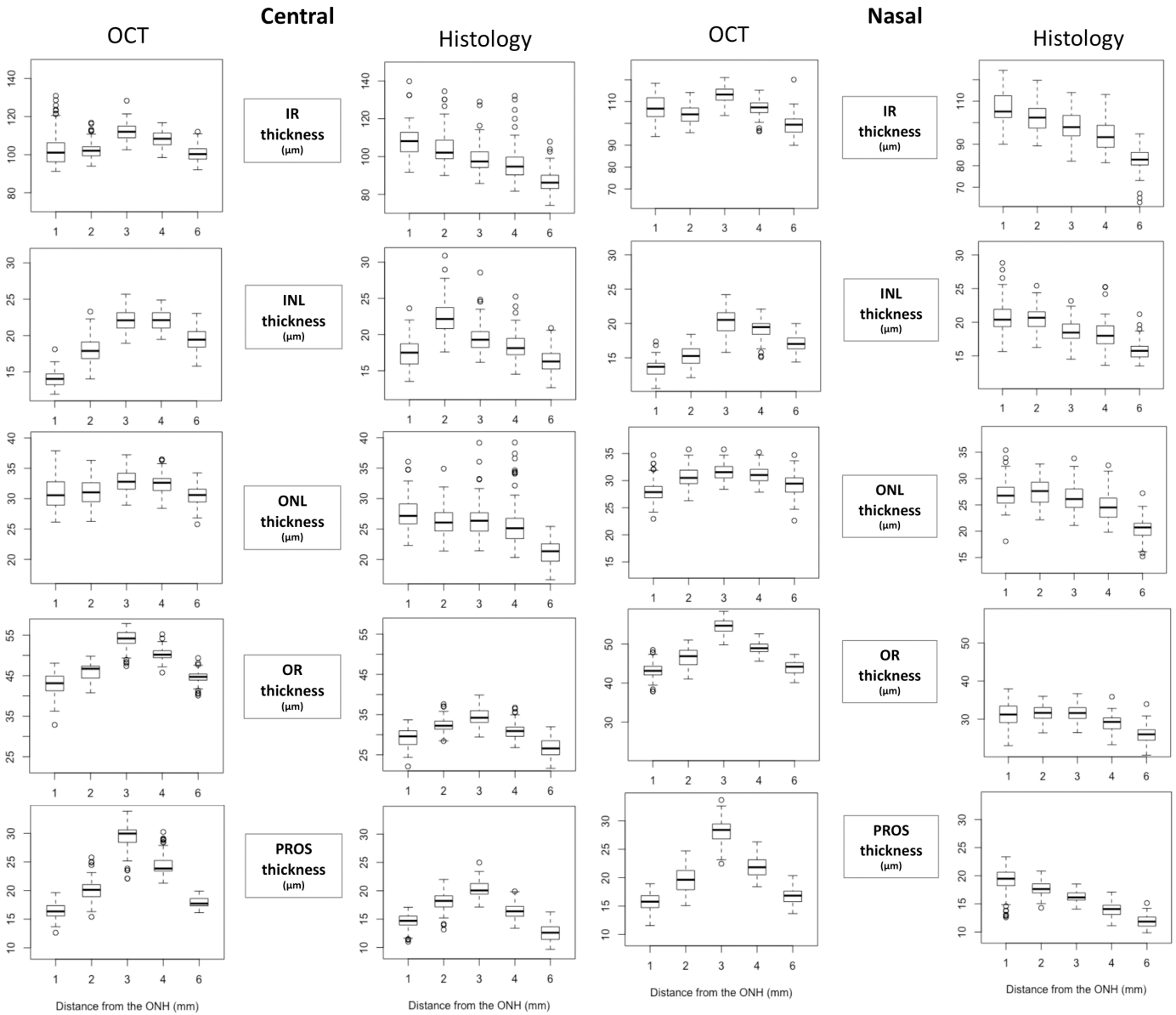


Figure 3. Retinal layer thickness on SD-OCT B-scans and histology sections through the visual streak and central ONH. All retinal thickness measurements obtained at 1, 2, 3, 4, and 6 mm ventral to the lower ONH rim in the central ONH location are presented as Boxplots. X-axes indicate the distance from the inferior edge of the ONH and Y-axes indicate the thickness of each layer/zone in μm . INL (inner nuclear layer); IR, inner retina; ONL, outer nuclear layer; OR, outer retina; PROS, photoreceptor outer segment length.

Figure 4. Retinal layer thickness on SD-OCT B-scans and histology sections through the visual streak and nasal ONH. All retinal thickness measurements obtained at 1, 2, 3, 4, and 6 mm ventral to the lower ONH rim in the nasal ONH location are presented as Boxplots. X-axes indicate the distance from the inferior rim of the ONH and Y-axes indicate the thickness of each layer/zone in μm . INL (inner nuclear layer); IR, inner retina; ONL, outer nuclear layer; OR, outer retina; PROS, photoreceptor outer segment length.

Histology-derived OR and PROS thickness measurements at the nasal rim of the ONH demonstrated significant discrepancies compared to the OCT-derived measurements. The PROS layer was longest at the 1 mm position and progressively shortened with increasing distance from the ventral ONH rim. Outer retinal thickness showed no statistically significant differences at the 1, 2, and 3 mm positions

and then decreased significantly at the 4 mm and again at the 6 mm positions.

Inner Retinal Layers

With some variations in significance levels, IR, INL, and ONL thickness measured on OCT at the central and nasal ONH followed a similar trend as OR and PROS thickness with all layers thickest in the center of the VS and thinnest outside the VS. Histology-derived

Table. Method Comparison Results

Measured Layers/Zones	Evidence of Differences between OCT and Histology Rejection of Null Hypothesis at $P < 0.05$				Repeatability Coefficient (rc)	
	Inter-Method Bias		Precision P Value	Repeatability P Value	rcOCT	rcHisto
	Value \pm SE	P Value				
IR	7.8 \pm 0.77	<0.0001	0.57	<0.0001	9.7	25.7 (+165%)
INL	-0.71 \pm 0.27	0.0079	0.98	<0.0001	5.4	9.2 (+70%)
ONL	5.3 \pm 0.33	<0.0001	0.36	<0.0001	5.2	7.7 (+48%)
OR	17.3 \pm 0.23	<0.0001	0.056	<0.0001	4.9	9.7 (+98%)
PROS	4.9 \pm 0.25	<0.0001	0.0019	<0.0001	4.7	11.1 (+136%)

Linear mixed effects models were used to evaluate whether differences between OCT and histology exist regarding the measurement means, between-subject variance and within-subject variance of retinal layer/zone thickness measurements. The null hypothesis stated that the measurement means (inter-method bias), between-subject variance (precision) and the within-subject variance (repeatability) are equal for both measurement methods. Inter-method bias is presented as value \pm standard error and represents the difference between the means of the two methods.

IR, INL, and ONL thickness tended to be thickest at the 1 or 2 mm position and progressively thinner with increasing distance from the ventral ONH rim. This trend is similar to the histology-derived OR and PROS thicknesses at the nasal ONH rim, but is notably different from histology-derived OR and PROS thicknesses at the center of the ONH.

Comparison of OCT and Histology as Measurement Methods

The results of the comparison of the two measurement methods, OCT and histology, using linear mixed effects models are presented in the Table. This study demonstrated that, overall, the means of IR, ONL, OR and PROS thickness measurements collected via histology were significantly lower than via OCT ($P < 0.0001$). The means of INL thickness measurements collected via histology were significantly higher than via OCT ($P = 0.0079$). These results demonstrate the inter-method bias between OCT and histology as measurement methods. Furthermore, OCT and histology-based thickness measurements yielded equal between-subject variances (precision) for all measured layers, except for the PROS measurements. OCT-based PROS measurements tended to be more precise than histology-based PROS measurements ($P = 0.0019$). Finally, OCT-based thickness measurements had a significantly lower within-subject variance (repeatability) for all measured layers compared with histology-based measurements ($P < 0.0001$), as illustrated by the repeatability coefficients (Table). OCT thus has a better repeatability than histology.

Total and Outer Retinal Thickness Topography

A line segmentation of complete 12 \times 12 mm OCT volume scans from three rabbits was performed to illustrate the TRT and OR thickness and the extent of the VS across the scanned area. Figure 5 represents the total and outer retinal thickness topography for one rabbit eye. The OR thickness topography highlighted the increased OR thickness within the rabbit VS and the extent of the rabbit VS (Fig. 5E). Of all OR bands, the most profoundly thickened band within the VS was the hyporeflexive photoreceptor outer segment band (Figs. 5C and 5D). The TRT topography showed two areas of increased thickness, one corresponding to the VS and the second lining up with the myelinated ganglion cell axons of the rabbit medullary rays at the dorsal edge of the topography (Fig. 5F). The total and outer retinal thickness topographies from all three rabbits were comparable (Supplementary Figure S3).

Ganglion Cell and INL and ONL Row Counts on Central Histology Sections

GC counts demonstrated a clear peak in GC density within the VS at 2 mm ventral to the ONH rim. The GC density progressively decreased towards the periphery (Fig. 6A). The number of rows of INL nuclei was also greatest within the VS at 2 mm ventral to the ONH rim and also showed a progressive decrease in number toward the periphery. INL nuclei row number was lowest outside the VS at the 6 mm position (Fig. 6B). The number of rows of ONL nuclei

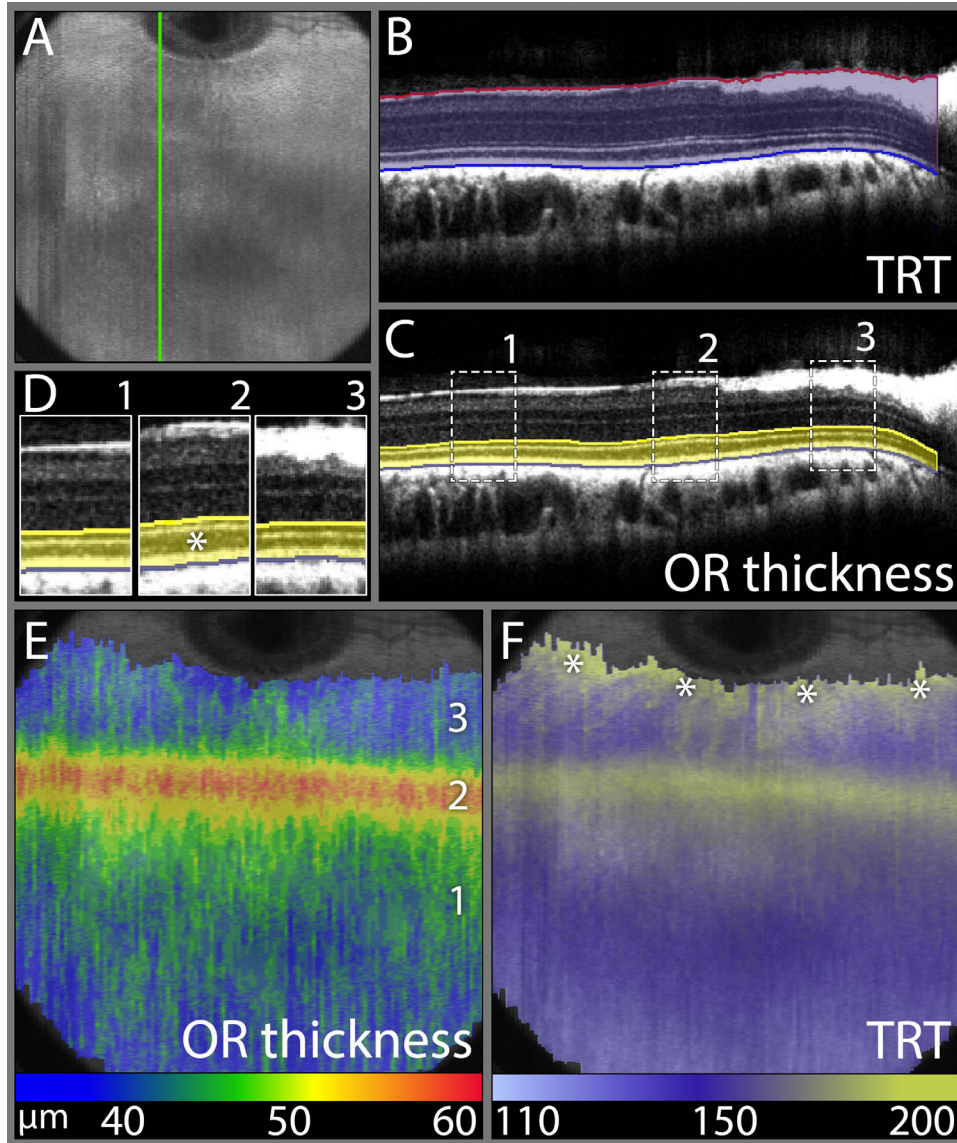


Figure 5. Total and outer retinal thickness topography demonstrating the extent of the rabbit visual streak. (A) OCT volume intensity projection image presenting an overview of a rabbit fundus corresponding to the retinal region imaged with a 12×12 mm volume scan. (B) SD-OCT B-scan along the green line in panel A illustrating the manually assisted segmentation of the ILM-vitreous interface and RPE/BM-choriocapillaris interface to obtain a total retinal thickness (TRT) topography. (C) SD-OCT B-scan along the green line in panel A illustrating the manually assisted segmentation of the ELM line and RPE/BM-choriocapillaris interface to obtain an outer retinal (OR) thickness topography. (D) Magnified and juxtapositioned sections of three different locations indicated in panel (C). Zone 2 is in the center of the visual streak and is easily recognized by the thickened hyporeflective outer segment band (*), compared to zones 1 and 3, which lie outside the visual streak. (E) OR thickness topography projected onto the OCT volume intensity projection image from panel A. This image demonstrates a horizontal band of increased OR thickness at 3mm ventral to the ventral ONH rim and centered over zone 2 from panels C and D, which demonstrates the increased thickness of the outer retina in and the extent of the rabbit visual streak. (F) TRT topography projected onto the OCT volume intensity projection image demonstrating two areas of increased thickness, one corresponding to the VS on the OR thickness topography and the second indicating the ventrally directed medullary rays at the dorsal image edge (asterisks). False color scales are used to indicate OR thickness and TRT in μm in panels E and F, respectively.

was greatest within the visual streak at 2 and 3 mm ventral to the ONH rim and lowest in the periphery outside the VS at the 6mm position (Fig. 6C). Numerical values of the manual cell counting and corresponding *P* values for all comparisons

are presented in Supplementary Tables S3a and S3b, respectively.

These results fit with the central OCT B-scan thickness measurements and with most of the central histology section thickness measurements.

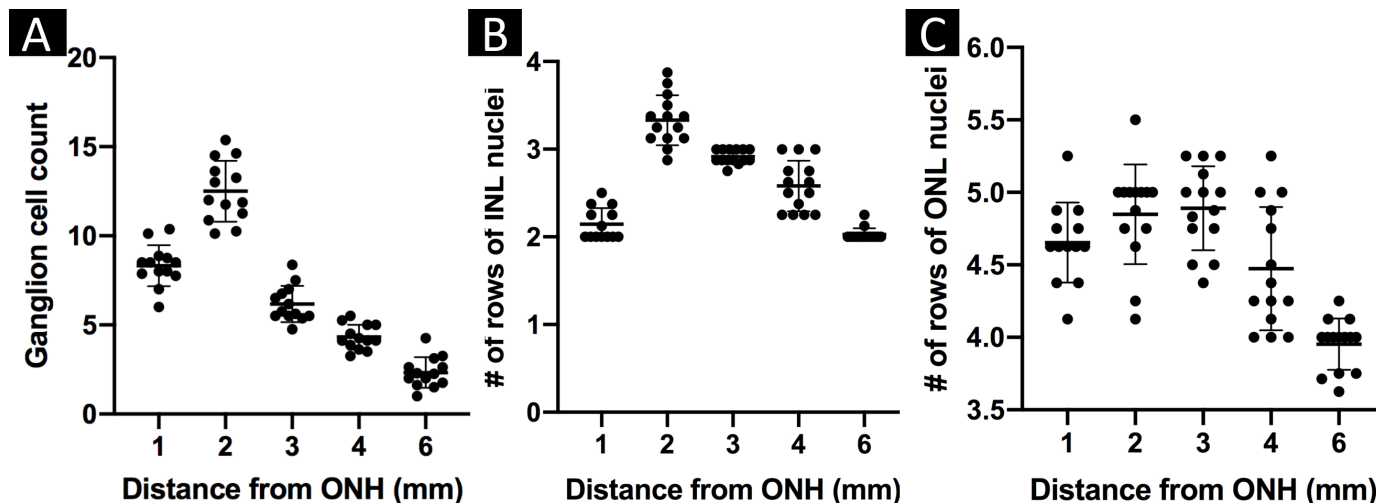


Figure 6. Histologic ganglion cell counts and INL and ONL row counts in- and outside of the central visual streak. Manual counts of the numbers of ganglion cells (A) and of the numbers of rows of INL (B) and ONL (C) nuclei visible per high power field (40 \times) in vertical histology sections transecting the central visual streak and ONH were presented as separate scatter plots with the mean counts per animal plotted for each location. The horizontal bars show the location means and the error bars the standard deviations. INL, inner nuclear layer; ONL, outer nuclear layer.

Semithin Resin Histology

Semithin sections were evaluated to visualize the photoreceptor outer segment length inside and outside of the VS. The resin sections demonstrated the greatest PROS length at 2.5 mm ventral to the ONH rim and decreasing PROS length on either side of this maximum (Fig. 7C). These findings agree with central hematoxylin and eosin section and nasal and central OCT scan findings.

Discussion

The present study demonstrates that OCT examination is possible in awake rabbits with reliable separation and identification of retinal layers enabling retinal layer thickness measurements. This is likely facilitated by the fact that rabbits, especially when mildly restrained, display very little spontaneous oculomotor activity in contrast to animals with well-developed foveal vision (such as dogs, cats, non-human primates, and humans).⁵⁸ Also, habituation to personnel and towel wrap restraining avoids stress reactions when performing noninvasive procedures like OCT. Thus, rabbits do not necessarily have to undergo anesthesia for each OCT examination, saving both time and resources and facilitating repeat OCT examinations in longitudinal studies. In line with 3R principles, such measures can both improve animal welfare and help to reduce research animal numbers.^{59,60} Moreover, the

rabbit is considered a risk species for anesthetic complications which increases the impact of removing or decreasing the burden of anaesthesia from the experimental design.^{61,62}

Our OCT-histology comparisons demonstrate that the VS is best defined on OCT as a 2 mm wide horizontal band centered 3 mm below the ventral ONH rim (Fig. 5 and Supplementary Figure S3). The VS can be identified on SD-OCT by the clearly visible increased thickness of the OR in the VS, especially the hyporeflexive photoreceptor OS band (Fig. 5). Quantitative data on normal rabbit retinal anatomy generated via SD-OCT under general anesthesia have been reported in earlier studies but anatomical differences between the VS and surrounding retina were not described.⁴⁵⁻⁴⁷ Bartuma et al. reported TRT measurements at three positions centered around 6 mm ventral to the inferior margin of the ONH.³² The reported TRTs progressively decreased toward the periphery, which is in line with our results because regions dorsal to and in the center of the visual streak were not included in the measurements recorded by Bartuma et al.

Discrepancies between retinal thickness measurements on SD-OCT and histologic sections were observed in our study. Overall, measured layers were significantly thinner in paraffin sections compared with OCT. This was likely because of tissue shrinkage or retraction during histological processing.⁶³⁻⁶⁵ We observed areas with artifactually crushed or torn photoreceptor outer segments in the VS (Supplementary Figure S2) despite the use of Davidson's fixative

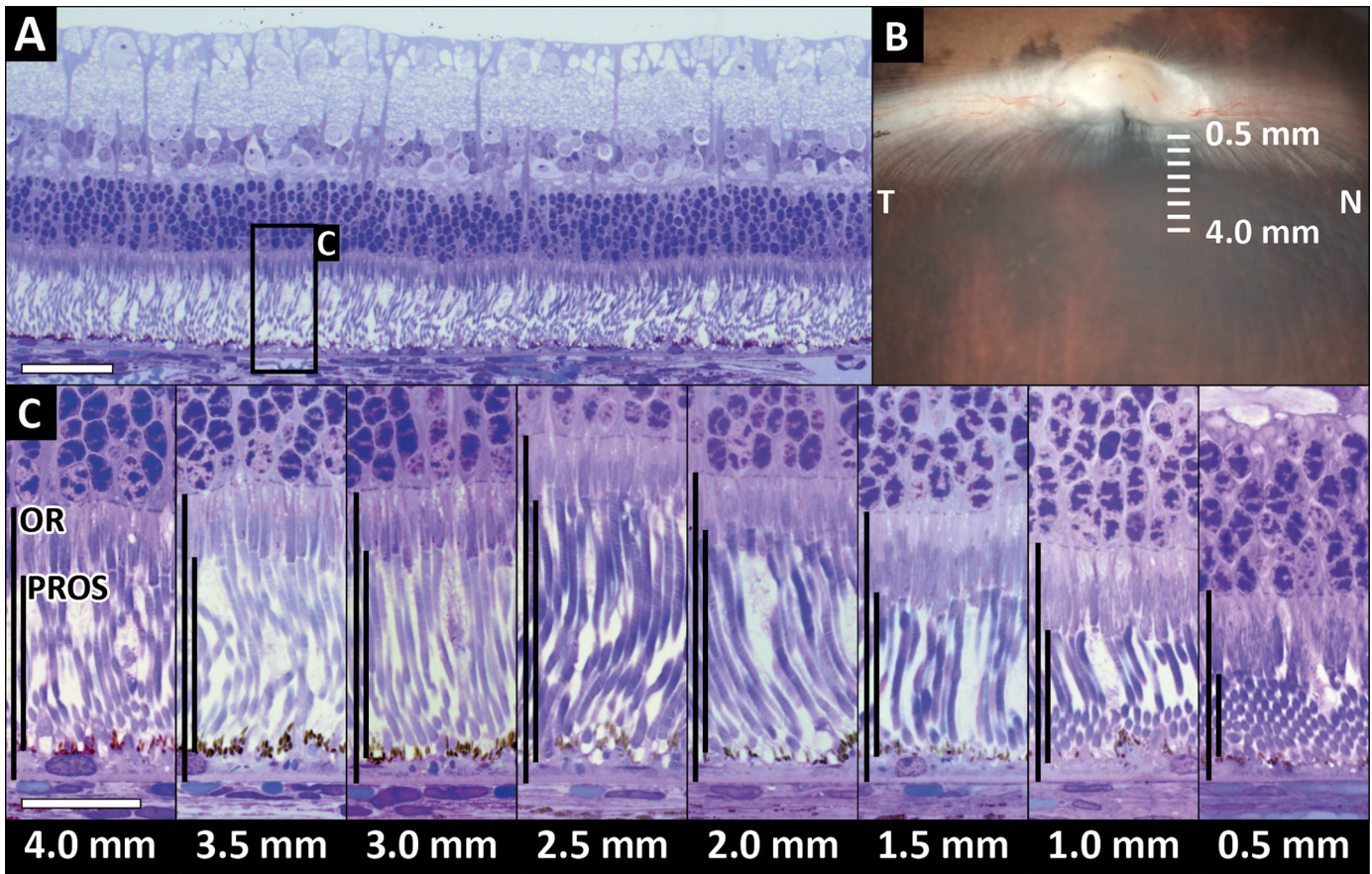


Figure 7. Semithin section histology: comparison of outer retina (OR) and photoreceptor outer segment length (PROS) at distances 0.5 mm to 4 mm ventral to the ONH. (A) Overview of a toluidine-blue stained semithin resin section of the retina at 3.5 mm ventral to the ONH. The black rectangle indicates the location of the detailed cutouts in panel C. (B) Image from dissection microscope illustrating location and orientation of the tissue sections. (C) The photoreceptor outer segments were longest at 2.5 mm ventral to the ONH where the perceived PROS:OR ratio was the highest. The lowest PROS:OR ratio was close to the ONH where the photoreceptor inner segments were longer and the outer segments were shorter than in the visual streak. N, nasal; T, temporal. Section thickness: 750 μm . Horizontal scale bar = 50 μm (A), 20 μm (C).

solution, known to provide excellent preservation of retinal tissue and to prevent retinal detachment in rabbits (Shariati A, et al. IOVS 2008;49:ARVO E-Abstract 5207). Similarly, other authors found that a direct comparison of retinal thicknesses obtained from histological sections and in vivo SD-OCT images was difficult because of artifacts in paraffin sections related to fixation and processing methods.^{23,66–68} The authors therefore believe that the obvious discrepancies in OR and PROS measurements between nasal paraffin sections and other measurements are due to processing artifacts. The semithin sections from nasal glutaraldehyde fixed, resin-embedded tissue samples confirmed this hypothesis by demonstrating the greatest PROS length at 2.5 mm ventral to the nasal ONH rim (Fig. 7C). A position estimation inaccuracy of ± 0.5 mm is possible due to the resin block cutting technique. Therefore, the nasal resin section histology,

the nasal and central OCTs and the central paraffin section histology all identified the greatest PROS length at the center of the visual streak roughly 3 mm below the ONH rim.

All paraffin section measurements demonstrated increased inner retinal layer thicknesses close to the ONH rim which were not identified on the OCT scans. We observed that the physiologic deep optic nerve cup present in rabbits is much less pronounced on histological sections, thus potentially creating retinal thickness increases near the ONH. Meredith et al. demonstrated that IOP in human patients may be important in maintaining structural integrity of the cribriform plate and ONH.⁶⁹ We therefore believe that a sudden postmortem decrease of IOP caused by globe enucleation might have caused the reduction of optic cup volume and artifactual increase of inner retinal layer thickness observed on our paraffin sections. This

clearly highlights the significant advantage of SD-OCT imaging over histological techniques for the collection of precise axial quantitative data, free of the aforementioned artifacts. The statistical comparison of both methods used in the present study, OCT and histology, also demonstrated that OCT and histology should not be used interchangeably and that OCT should be the favored choice to measure retinal layer thicknesses.

The present study has some limitations. First, all OCT and histology measurements were performed manually which is time-consuming and can introduce subjective bias. However, differences between graders were low in a random sample of OCT measurements (data not shown), which makes it unlikely that such a subjective bias would have influenced the measurement results. Second, although segmentation algorithms for human OCT scans can be used in animal research, their use may lead to segmentation errors.^{24,27} Extensive manual corrections were needed with the use of automated segmentation software in our study to generate accurate segmentation data. The three segmentation lines at the ILM-vitreous interface, ELM, and RPE/BM-choriocapillaris interface were individually verified, manually corrected, or completely retraced if necessary, in case of incorrect delineation. Third, measurements of lateral distances between measurement positions on the OCT scans might not be accurate since the dimensions of the rabbit eye, axial globe length and other biometric parameters differ from the human eye. The axial dimension of single OCT A-scan measurements is independent of the optical power of the eye and does not change after scaling for lateral magnification.^{24,70,71} Finally, the acquisition of sufficient quality OCT volume scans is possible in minimally restrained awake rabbits because of their low spontaneous oculomotor activity. High-resolution imaging of the retina has also successfully been performed in awake mice that were surgically fitted with a head-fixation device that provided exceptional ocular stability after a training period (Schallek JB, et al. IOVS 2018;59:ARVO E-Abstract 732). However, it is doubtful that these approaches will be equally successful in animals with well-developed foveal vision (such as dogs, cats, and non-human primates)⁵⁸, which limits the translation of these techniques to other large-animal models.

The results of this study demonstrate that SD-OCT is a reproducible, reliable, and noninvasive in vivo imaging technique that can yield high-quality images of the rabbit retina and allow identification of the VS without the need for general anesthesia. These qualities make SD-OCT ideal for use in experimental rabbits in clinical as well as experimental settings.

Acknowledgments

The authors thank Martina Stirn for technical support with semithin section histology imaging and Elisa Mischi for providing a design template for Supplementary Figure S1.

Disclosure: **A. Lavaud**, None; **P. Soukup**, None; **L. Martin**, None; **S. Hartnack**, None; **S. Pot**, None

References

1. Famiglietti EV, Sharpe SJ. Regional topography of rod and immunocytochemically characterized “blue” and “green” cone photoreceptors in rabbit retina. *Vis Neurosci*. 1995;12:1151–1175.
2. Rockhill RL, Daly FJ, MacNeil MA, Brown SP, Masland RH. The diversity of ganglion cells in a mammalian retina. *J Neurosci*. 2002;22:3831–3843.
3. Vaney DI, Gynther IC, Young HM. Rod-signal interneurons in the rabbit retina: 2. AII amacrine cells. *J Comp Neurol*. 1991;310:154–169.
4. Young HM, Vaney DI. Rod-signal interneurons in the rabbit retina: 1. Rod bipolar cells. *J Comp Neurol*. 1991;310:139–153.
5. Juliusson B, Bergstrom A, Rohlich P, Ehinger B, van Veen T, Szel A. Complementary cone fields of the rabbit retina. *Invest Ophthalmol Vis Sci*. 1994;35:811–818.
6. Peiffer RL, Pohm-Thorsen L, Corcoran K. Models in ophthalmology and vision research. In: Manning PJ, Ringler DH, Newcomer CE (Eds.), *The Biology of the Laboratory Rabbit (Second Edition)*. San Diego: Academic Press; 1994:409–433.
7. Qiu G, Stewart JM, Sada S, et al. A new model of experimental subretinal neovascularization in the rabbit. *Exp Eye Res*. 2006;83:141–152.
8. Kondo M, Sakai T, Komeima K, et al. Generation of a transgenic rabbit model of retinal degeneration. *Invest Ophthalmol Vis Sci*. 2009;50:1371–1377.
9. Yamauchi Y, Agawa T, Tsukahara R, et al. Correlation between high-resolution optical coherence tomography (OCT) images and histopathology in an iodoacetic acid-induced model of retinal degeneration in rabbits. *Br J Ophthalmol*. 2011;95:1157–1160.
10. Li K, Liu S, Zhong X, Ge J. Generation of an acute retinal photoreceptor degeneration model in rabbits. *Am J Transl Res*. 2018;10:235–245.
11. de Zafra CLZ, Sasseville VG, Matsumoto S, et al. Inflammation and immunogenicity limit the utility of the rabbit as a nonclinical species for ocular

- biologic therapeutics. *Regul Toxicol Pharmacol.* 2017;86:221–230.
12. Vaney DI, Young HM, Gynther IC. The rod circuit in the rabbit retina. *Vis Neurosci.* 1991;7:141–154.
 13. Vaney DI, Levick WR, Thibos LN. Rabbit retinal ganglion cells. Receptive field classification and axonal conduction properties. *Exp Brain Res.* 1981;44:27–33.
 14. Vaney DI, Hughes A. The rabbit optic nerve: fibre diameter spectrum, fibre count, and comparison with a retinal ganglion cell count. *J Comp Neurol.* 1976;170:241–251.
 15. Oyster CW, Takahashi ES, Hurst DC. Density, soma size, and regional distribution of rabbit retinal ganglion cells. *J Neurosci.* 1981;1:1331–1346.
 16. Davis FA. The anatomy and histology of the eye and orbit of the rabbit. *Trans Am Ophthalmol Soc.* 1929;27:402–441.
 17. Levick WR. Receptive fields and trigger features of ganglion cells in the visual streak of the rabbits retina. *J Physiol.* 1967;188:285–307.
 18. Chievitz JH. Über das Vorkommen der Area centralis retinae in den vier höheren Wirbeltierklassen. *Arch Anat Physiol Lpz Anat A.* 1891;139:311–334.
 19. Hughes A. Topographical relationships between the anatomy and physiology of the rabbit visual system. *Doc Ophthalmol.* 1971;30:33–159.
 20. Chen TC, Cense B, Pierce MC, et al. Spectral domain optical coherence tomography: ultra-high speed, ultra-high resolution ophthalmic imaging. *Arch Ophthalmol.* 2005;123:1715–1720.
 21. Srinivasan VJ, Monson BK, Wojtkowski M, et al. Characterization of outer retinal morphology with high-speed, ultrahigh-resolution optical coherence tomography. *Invest Ophthalmol Vis Sci.* 2008;49:1571–1579.
 22. Spaide RF, Curcio CA. Anatomical correlates to the bands seen in the outer retina by optical coherence tomography: literature review and model. *Retina.* 2011;31:1609–1619.
 23. Berger A, Cavallero S, Dominguez E, et al. Spectral-domain optical coherence tomography of the rodent eye: highlighting layers of the outer retina using signal averaging and comparison with histology. *PloS one.* 2014;9:e96494.
 24. Dysli C, Enzmann V, Sznitman R, Zinkernagel MS. Quantitative analysis of mouse retinal layers using automated segmentation of spectral domain optical coherence tomography images. *Transl Vis Sci Technol.* 2015;4:9.
 25. Strouthidis NG, Grimm J, Williams GA, Cull GA, Wilson DJ, Burgoyne CF. A comparison of optic nerve head morphology viewed by spectral domain optical coherence tomography and by serial histology. *Invest Ophthalmol Vis Sci.* 2010;51:1464–1474.
 26. Koinzer S, Saeger M, Hesse C, et al. Correlation with OCT and histology of photocoagulation lesions in patients and rabbits. *Acta Ophthalmol.* 2013;91:e603–611.
 27. Soukup P, Maloca P, Altmann B, Festag M, Atzpodien EA, Pot S. Interspecies variation of outer retina and choriocapillaris imaged with optical coherence tomography. *Invest Ophthalmol Vis Sci.* 2019;60:3332–3342.
 28. Chen J, Qian H, Horai R, Chan CC, Caspi RR. Use of optical coherence tomography and electroretinography to evaluate retinal pathology in a mouse model of autoimmune uveitis. *PloS one.* 2013;8:e63904.
 29. Rosolen SG, Riviere ML, Lavillegrand S, Gautier B, Picaud S, LeGargasson JF. Use of a combined slit-lamp SD-OCT to obtain anterior and posterior segment images in selected animal species. *Vet Ophthalmol.* 2012;15(Suppl. 2):105–115.
 30. Gloesmann M, Hermann B, Schubert C, Sattmann H, Ahnelt PK, Drexler W. Histologic correlation of pig retina radial stratification with ultrahigh-resolution optical coherence tomography. *Invest Ophthalmol Vis Sci.* 2003;44:1696–1703.
 31. Cho BJ, Seo JM, Yu HG, Chung H. Monocular retinal degeneration induced by intravitreal injection of sodium iodate in rabbit eyes. *Jpn J Ophthalmol.* 2016;60:226–237.
 32. Bartuma H, Petrus-Reurer S, Aronsson M, Westman S, Andre H, Kvanta A. In vivo imaging of subretinal bleb-induced outer retinal degeneration in the rabbit. *Invest Ophthalmol Vis Sci.* 2015;56:2423–2430.
 33. Zhang QX, Lu RW, Messinger JD, Curcio CA, Guarcello V, Yao XC. In vivo optical coherence tomography of light-driven melanosome translocation in retinal pigment epithelium. *Sci Rep.* 2013;3:2644.
 34. Li T, Zhou XD, Luo X, Jiang B. Optical coherence tomography and histologic measurements of retinal and choroidal thicknesses in guinea pig eyes. *Int J Clin Exp Med.* 2016;9:7080–7087.
 35. Sajdak BS, Salmon AE, Litts KM, et al. Evaluating seasonal changes of cone photoreceptor structure in the 13-lined ground squirrel. *Vision Res.* 2019;158:90–99.
 36. Huang D, Swanson EA, Lin CP, et al. Optical coherence tomography. *Science.* 1991;254:1178–1181.
 37. Hernandez-Merino E, Kecova H, Jacobson SJ, Hamouche KN, Nzokwe RN, Grozdanic SD. Spectral domain optical coherence tomography

- (SD-OCT) assessment of the healthy female canine retina and optic nerve. *Vet Ophthalmol.* 2011;14:400–405.
38. Costa RA, Calucci D, Skaf M, et al. Optical coherence tomography 3: automatic delineation of the outer neural retinal boundary and its influence on retinal thickness measurements. *Invest Ophthalmol Vis Sci.* 2004;45:2399–2406.
 39. Chen TC, Cense B, Miller JW, et al. Histologic correlation of in vivo optical coherence tomography images of the human retina. *Am J Ophthalmol.* 2006;141:1165–1168.
 40. Staurengi G, Sadda S, Chakravarthy U, Spaide RF, International Nomenclature for Optical Coherence Tomography. Proposed lexicon for anatomic landmarks in normal posterior segment spectral-domain optical coherence tomography: the IN*OCT consensus. *Ophthalmology.* 2014;121:1572–1578.
 41. Huber G, Beck SC, Grimm C, et al. Spectral domain optical coherence tomography in mouse models of retinal degeneration. *Invest Ophthalmol Vis Sci.* 2009;50:5888–5895.
 42. Oishi A, Hata M, Shimozono M, Mandai M, Nishida A, Kurimoto Y. The significance of external limiting membrane status for visual acuity in age-related macular degeneration. *Am J Ophthalmol.* 2010;150:27–32 e21.
 43. Muraoka Y, Ikeda HO, Nakano N, et al. Real-time imaging of rabbit retina with retinal degeneration by using spectral-domain optical coherence tomography. *PLoS one.* 2012;7:e36135.
 44. Fujimoto JG. Optical coherence tomography for ultrahigh resolution in vivo imaging. *Nat Biotechnol.* 2003;21:1361–1367.
 45. Ge J, Luo R, Guo Y. Corrective change of retinal thickness measured by optical coherence tomography and histologic studies. *Yan Ke Xue Bao.* 1999;15:153–155, 178.
 46. Alkin Z, Kashani AH, Lopez-Jaime GR, Ruiz Garcia H, Humayun MS, Sadda SR. Quantitative analysis of retinal structures using spectral domain optical coherence tomography in normal rabbits. *Curr Eye Res.* 2013;38:299–304.
 47. Carpenter CL, Kim AY, Kashani AH. Normative retinal thicknesses in common animal models of eye disease using spectral domain optical coherence tomography. *Adv Exp Med Biol.* 2018;1074:157–166.
 48. McLellan GJ, Rasmussen CA. Optical coherence tomography for the evaluation of retinal and optic nerve morphology in animal subjects: practical considerations. *Vet Ophthalmol.* 2012;15(Suppl. 2):13–28.
 49. de Oliveira Dias JR, Badaro E, Novais EA, et al. Preclinical investigations of intravitreal ziv-aflibercept. *Ophtha Surg Lasers Imaging Retina.* 2014;45:577–584.
 50. Dubielzig R, Ketrting K, McLellan G, Albert D. The principles and practice of ocular pathology. *Veterinary Ocular Pathology: A Comparative Review.* London: Elsevier Health Sciences, UK; 2010:1–8.
 51. Schneider CA, Rasband WS, Eliceiri KW. NIH Image to ImageJ: 25 years of image analysis. *Nat Methods.* 2012;9:671–675.
 52. Mayer M. *Automated glaucoma detection with optical coherence tomography.* Friedrich-Alexander-Universitaet Erlangen-Nuernberg; 2018:132, accessed at: <https://opus4.kobv.de/opus4-fau/frontdoor/index/index/year/2018/docId/9849>.
 53. Hothorn T, Bretz F, Westfall P. Simultaneous inference in general parametric models. *Biom J.* 2008;50:346–363.
 54. Pinheiro J, Bates D, DebRoy S, Sarkar D, R Core Team. *nlme: Linear and Nonlinear Mixed Effects Models.* 2019.
 55. R Core Team. *R: A Language and Environment for Statistical Computing.* Vienna, Austria: R Foundation for Statistical Computing.; 2019.
 56. Roy A. An application of linear mixed effects model to assess the agreement between two methods with replicated observations. *J Biopharm Stat.* 2009;19:150–173.
 57. Bland JM, Altman DG. Measuring agreement in method comparison studies. *Stat Methods Med Res.* 1999;8:135–160.
 58. Collewijn H, van der Mark F. Ocular stability in variable visual feedback conditions in the rabbit. *Brain Res.* 1972;36:47–57.
 59. Hawkins P, Hubrecht R, Buckwell A, et al. *Refining rabbit care: A resource for those working with rabbits in research.* RSPCA; 2008, accessed at: <https://science.rspca.org.uk/documents/1494935/9042554/Refining+rabbit+care+-+report.pdf/a528fbaa-f11a-a5ff-f3e3-38e6e6439f4d?t=1552901950204>.
 60. Heindl C, Hess A, Brune K. Refinement and reduction in animal experimentation: options for new imaging techniques. *ALTEX.* 2008;25:121–125.
 61. Brodbelt DC, Blissitt KJ, Hammond RA, et al. The risk of death: the confidential enquiry into perioperative small animal fatalities. *Vet Anaesth Analg.* 2008;35:365–373.
 62. Lee HW, Machin H, Adami C. Peri-anaesthetic mortality and nonfatal gastrointestinal complications in pet rabbits: a retrospective study on 210 cases. *Vet Anaesth Analg.* 2018;45:520–528.

63. Margo CE, Lee A. Fixation of whole eyes: the role of fixative osmolarity in the production of tissue artifact. *Graefes Arch Clin Exp Ophthalmol*. 1995;233:366–370.
64. Fukuchi T, Takahashi K, Uyama M, Matsumura M. Comparative study of experimental choroidal neovascularization by optical coherence tomography and histopathology. *Jpn J Ophthalmol*. 2001;45:252–258.
65. Jiao J, Mo B, Wei H, Jiang YR. Comparative study of laser-induced choroidal neovascularization in rats by paraffin sections, frozen sections and high-resolution optical coherence tomography. *Graefes Arch Clin Exp Ophthalmol*. 2013;251:301–307.
66. Anger EM, Unterhuber A, Hermann B, et al. Ultrahigh resolution optical coherence tomography of the monkey fovea. Identification of retinal sublayers by correlation with semithin histology sections. *Exp Eye Res*. 2004;78:1117–1125.
67. Srinivasan VJ, Ko TH, Wojtkowski M, et al. Non-invasive volumetric imaging and morphometry of the rodent retina with high-speed, ultrahigh-resolution optical coherence tomography. *Invest Ophthalmol Vis Sci*. 2006;47:5522–5528.
68. Knott EJ, Sheets KG, Zhou Y, Gordon WC, Bazan NG. Spatial correlation of mouse photoreceptor-RPE thickness between SD-OCT and histology. *Exp Eye Res*. 2011;92:155–160.
69. Meredith SP, Swift L, Eke T, Broadway DC. The acute morphologic changes that occur at the optic nerve head induced by medical reduction of intraocular pressure. *J Glaucoma*. 2007;16:556–561.
70. Lozano DC, Twa MD. Development of a rat schematic eye from in vivo biometry and the correction of lateral magnification in SD-OCT imaging. *Invest Ophthalmol Vis Sci*. 2013;54:6446–6455.
71. Sanchez-Cano A, Baraibar B, Pablo LE, Honrubia FM. Magnification characteristics of the optical coherence tomograph STRATUS OCT 3000. *Ophthalmic Physiol Opt*. 2008;28:21–28.